Photoinduced magnetization in dilute magnetic (semimagnetic) semiconductors

H. Krenn and K. Kaltenegger
Institut für Physik, Montanuniversität Leoben, A-8700 Leoben, Austria

T. Dietl
Institute of Physics, Polish Academy of Sciences, aleja Lotnikow 32/46, PL-02668 Warszawa, Poland

J. Spałek*
Department of Physics, Purdue University, West Lafayette, Indiana 47907

G. Bauer
Institut für Physik, Montanuniversität Leoben, A-8700 Leoben, Austria
(Received 18 November 1988)

Optically induced magnetization was studied in narrow-gap $Hg_{1-x}Mn_xTe$ in zero external magnetic field as a function of composition, excitation energy, and temperature. These experimental results, together with previously published data for $Hg_{1-x}Mn_xTe$ as well as for $Cd_{1-x}Mn_xTe$ [Awschalom *et al.*, Phys. Rev. Lett. **58**, 812 (1987)] are analyzed. Two mechanisms of Mn-spin orientation by photoelectrons brought about by the *s-d* coupling are considered: (i) the static polarization induced by the mean field of spin-polarized electrons, and (ii) the dynamic polarization caused by the *s-d* spin-flip scattering. The analysis implies the dynamic polarization to be strongly suppressed by interaction among the Mn spins. In the case of $Hg_{1-x}Mn_xTe$ the static polarization is calculated to be in quantitative agreement with the measured photomagnetization. In the wide-gap $Cd_{1-x}Mn_xTe$ a comparatively small value of the observed photomagnetization implies the presence of an efficient spin relaxation of photoelectrons, presumably related to trapping by bound states. In order to describe the dependence of photomagnetization on excitation energy, the energy loss of photoinjected carriers by LO-phonon emission was considered. In addition to spin relaxation of photoelectrons by magnetic ions, the decay of spin orientation caused by spin-orbit coupling was taken into account. The latter effect is particularly strong in the narrow-gap case. The model correctly reproduces a strong dependence of photomagnetization on excitation energy in narrow-gap $Hg_{1-x}Mn_xTe$ and its absence in $Cd_{1-x}Mn_xTe$.

I. INTRODUCTION

The diluted magnetic (semimagnetic) semiconductors are a class of semiconducting materials which have become a subject of intensive experimental and theoretical investigations in recent years.[1–4] They combine the essential features of conventional semiconductors with interesting magnetic properties which can be tuned by composition and by external magnetic fields in a controlled manner. The spin-spin exchange interaction between the paramagnetic ions themselves and between these ions and the free carriers results in profound effects which have been investigated by many different techniques.

It has been recently shown by some of the present authors that a magnetization in zero external magnetic field can be induced by optically excited carriers in $Hg_{1-x}Mn_xTe$.[5,6] Novel techniques were employed, namely a combination of optical pumping, i.e., photoexcitation of carriers by circularly polarized light, with the detection of the minute, induced magnetization using a superconducting quantum-interference device (SQUID). Awschalom and co-workers[7,8] have improved this technique using SQUID's with a lower noise level and have studied via the optically induced magnetization in wide-gap $Cd_{1-x}Mn_xTe$ both the energetics and spin dynamics of the magnetic response on a picosecond time scale.

We have shown that the observed magnetization is due to the orientation of the Mn ions caused by the spin-polarized, excited electrons. In the same way the use of optical pumping techniques has substantially improved our knowledge on the spin-relaxation phenomena[9–14] of photoexcited free carriers, the photomagnetization effect in diluted magnetic semiconductors offers the potential of studying relaxation phenomena of the oriented Mn ions. Furthermore, the magnetic response of the samples can be studied as a function of excitation intensity, polarization, and temperature as well as of the photon energy. Since all the phenomena mentioned above depend crucially on the band structure of the materials, in Fig. 1 the energy levels close to the fundamental gap are shown for inverted, zero, and open-gap $Hg_{1-x}Mn_xTe$ as well as for the wide-gap material $Cd_{1-x}Mn_xTe$.

It is the purpose of this paper to address and clarify the fundamental question of how the spin-polarized free carriers orient the localized $3d$ electrons of the Mn ions. The exchange interaction as described by the *s-d* interaction Hamiltonian, $-J\mathbf{S}\cdot\mathbf{s}$, offers two possibilities.

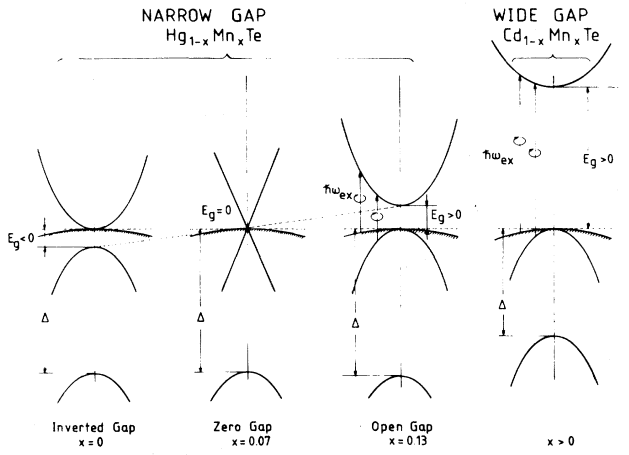

FIG. 1. Energy-band diagrams for semimagnetic semiconductors. In the materials where optically induced magnetization is observed the corresponding interband transitions are marked by arrows.

(i) The spin-polarized conduction electrons cause an effective field along the propagation direction of the exciting light (z direction) in which the Mn ions are oriented according to their low-field susceptibility $\chi(T)$. This polarization is produced by diagonal elements of the s-d interaction Hamiltonian and will be referred to as the mean-field effect.

(ii) The spin-polarized carriers can transfer their polarization to the Mn subsystem via a spin-flip mechanism. This type of interaction, the dynamic polarization, involves the off-diagonal elements of the s-d interaction Hamiltonian. Rather weak Mn-Mn spin interactions turn out to be necessary for the dynamic polarization to result in a sizable value.

There are already some well-known phenomena, such as the magnetic polarons in diluted magnetic semiconductors (DMS's), where the mean-field approach has proved to be insufficient and thermodynamic fluctuations of the spin field were shown to be important.[15–19] Some investigations, like the first report[5] on the light-induced magnetization in $Hg_{1-x}Mn_xTe$, have emphasized the importance of spin-flip–scattering effects.

In this paper we analyze the relative importance of both contributions to the total magnetization in zero external magnetic field. It is organized as follows: In Sec. II we describe the experimental setup for measurements on the narrow-gap material $Hg_{1-x}Mn_xTe$. In Sec. III the experimental results, namely the polarization, the temperature dependence, and the dependence on exciting photon energy of the light-induced magnetization, are shown. In Sec. IV a theoretical description follows, directed at the microscopic aspects of the problem: the initial polarization of spin-oriented electrons, their spin-spin exchange with the Mn $3d$ electrons, and the various relaxation phenomena of both subsystems. Next, in Sec. V, a comparison between results and the analysis of the effects in a narrow-gap system and the results of Awschalom and co-workers[7,8] for the wide-gap system $Cd_{1-x}Mn_xTe$ ($x=0.2$) is presented. A unifying treatment for both materials is possible, if the details of the band structure and their influence on the relaxation phenomena are considered. In Sec. VI we provide a more complete understanding of the alignment of Mn ions due to their interaction with the spin-oriented free carriers, including the spin mechanics and relaxation rates. It turns out that the Mn-Mn spin relaxation is of crucial importance to the dynamic polarization.

We show that our own results combined with those of Awschalom and co-workers[7,8] lead to the conclusion that, in general, the orientation of the $3d$ electrons of the Mn ions occurs via the mean-field mechanism and that the dynamic polarization through spin-flip scattering is restricted to rather specific experimental conditions.

II. EXPERIMENTAL SETUP

In order to measure the optically induced magnetization, it is necessary to combine in the experimental setup typical features of an optical pumping experiment[11–14] with sensitive detection of magnetization using a superconducting quantum-interference device.[20] For the optical experiment an interband excitation has to be performed using circularly polarized light (Fig. 2). For the samples under investigation, zero- and open-gap $Hg_{1-x}Mn_xTe$ with x values ranging from 0.07 to 0.135, a cw CO laser was chosen, the photon energy of which can be varied by an intracavity grating ($\hbar\omega_{ex}=220$–245 meV). Instead of using a rotating $\lambda/4$ plate, a photoelastic modulator (ZnSe) operating at 37 kHz varies the po-

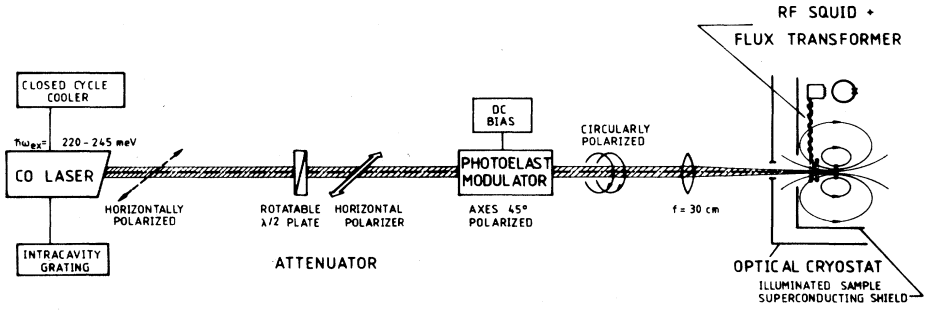

FIG. 2. Experimental setup: In an optical pumping experiment the degree of polarization of the CO-laser radiation is chopped by the photoelastic modulator from left to right circular polarization. The sample is located within a superconducting flux transformer of a rf SQUID.

larization by strain-induced birefringence. The principal strain axes are aligned at 45° with respect to the CO-laser-beam polarization (being linear in the horizontal plane). With appropriate setting of the modulator retardation, the incident linearly polarized light is chopped between left and right circular polarization within a modulation cycle. Particular attention is paid to the constant intensity of CO-laser radiation impinging on the sample in order to avoid any parasitic magnetic signals originating from thermal fluctuations within the sample.

In order to change the laser intensity on the sample, an attenuator arrangement is used consisting of a rotatable $\lambda/2$ plate and an AgBr linear polarizer. The radiation is focused onto the sample, which is mounted on a sample holder and surrounded by the pickup coil of the flux transformer providing an inductance of 2 μH, which is matched to the input coil of the toroidal radiofrequency SQUID. A niobium can is used to shield the SQUID system and the pickup coil from electromagnetic and static magnetic stray fields. A 2-mm-diam hole is drilled into the niobium shield so that the CO-laser radiation can impinge onto the sample. The whole area of the sample (0.8 mm diam) is illuminated in order to increase the magnetic coupling efficiency between the optically induced magnetic flux emerging from the sample and penetrating the pickup coil.

Apart from chopping the polarization between left- and right-circularly-polarized light at 37 kHz, a constant dc bias applied to the birefringent crystal enables us to check whether the magnetization signal vanishes for linearly polarized light.

Despite the hole in the niobium shield a SQUID signal is obtained with a noise limit which is as low as $(2\times10^{-4})\Phi_0/\sqrt{\text{Hz}}$; Φ_0 denotes the flux quantum ($\Phi_0=2.07\times10^{-15}$ V s). There is no observable degradation in comparison to a completely screened pickup coil in a closed niobium can. Since the superconducting shield provides excellent screening, no gradiometric flux transformer configuration with astatic coils was necessary. Since the absorption constant of $Hg_{1-x}Mn_xTe$ above the fundamental absorption edge is of the order of 10^4 cm^{-1}, the radiation is absorbed within approximately 1 μm, whereas the sample thickness is 0.5–1.0 mm. Thus the spin-polarized carriers which polarize the Mn ions form a sheet magnetically. The length of the pickup coil (0.5 mm, 3.5 mm diam) is large compared to the magnetic sheet, even taking electron and spin diffusion into consideration. The diffusion length of electrons is evaluated to be of the order of 10 μm, whereas that of localized spins is estimated to be at least 1 order of magnitude shorter. Under this condition the SQUID signal is proportional to the induced magnetic moment of the sample. It is very difficult to determine the actual coupling factor for the given geometrical arrangement of the sample and the pickup coil from calculations. Therefore, the coupling factor was determined experimentally: a single-turn coil with exactly the same size as the sample was placed in the pickup coil. It was found from the measured current through this coil and its area that the flux quantum Φ_0 picked up by the SQUID corresponded to the magnetic moment of 3.3×10^{-8} emu (4.1×10^{-17} T m^3).

Since the polarization chop rate is rather high (37 kHz) a compromise is necessary between the frequency response of the SQUID electronics and the minimum observable flux slewing rate. The detection limit of this system corresponds to a magnetic moment of 3.7×10^{-10} emu per $\sqrt{\text{Hz}}$ and per cm^2 (unit of sample area), and a slewing rate of $(3\times10^4)\Phi_0$/s.

The sample temperature can be varied independent of the SQUID system temperature within the limit 4–20 K, simply by changing the impinging laser power. Special care was taken to calibrate the temperature sensors to obtain reliable sample temperatures.

The $Hg_{1-x}Mn_xTe$ samples used were grown by a modified Bridgeman technique and annealed in Hg vapor. The hole concentration of about 10^{16} cm^{-3} is frozen out at liquid-helium temperatures, where practically no free carriers exist. Their x content was checked by x-ray diffraction. The $Hg_{1-x}Mn_xTe$ samples were cut into pieces of approximately $1\times1\times0.5$ mm^3, polished and etched with a bromine-methanol solution, and mounted into the pickup coil of the SQUID system. Due to the rapid variation of the energy gap with x content, any Hg diffusion within the top layer of about 1 μm thickness crucial for the optically induced magnetization signal has to be avoided. Therefore, the samples were directly immersed in liquid helium after the polishing and etching procedure.

Optically induced magnetization was detected also in a wide-gap material $Cd_{1-x}Mn_xTe$.[7,8] Awschalom and coworkers[7,8] have used a miniature dc SQUID susceptometer with integrated fiber optics to detect optically induced magnetization in $Cd_{1-x}Mn_xTe$ ($x=0.2$) with a pickup loop of 12×12 μm^2 (sample size: 10 μm diam, 1 μm thickness). In their experimental arrangement Φ_0 corresponded to a magnetic moment of 5.58×10^{-11} emu,[7] while detection limit per cm^2 (1.1×10^{-10} emu/cm$^2\sqrt{\text{Hz}}$) is comparable to ours. A magnetic moment of $\simeq8\times10^{-15}$ emu was detected[7] at 4.2 K for a laser power density of 5 kW/cm^2, corresponding to the light-induced bulk magnetization $\simeq10^{-4}$ emu. A magnetic field of $\simeq0.2$ Oe would produce such magnetization in $Cd_{0.8}Mn_{0.2}Te$ at 4.2 K.

III. EXPERIMENTAL RESULTS

For the $Hg_{1-x}Mn_xTe$ samples with x contents of about $x=0.07$, 0.11, 0.12, and 0.135, the induced flux as a function of the modulator retardation is shown in Fig. 3. It is seen that no detectable magnetization is observed within our noise limit for the zero-gap material ($x=0.07$). For larger Mn concentrations (energy gap) the signal was detected and found to attain the maximum value for circularly polarized radiation. A strong sensitivity of photomagnetization on the energy gap demonstrates that the effect is *not* caused by a direct influence of the light on *d* electrons. Furthermore, no photomagnetization was found in nonmagnetic InSb and $Hg_{0.77}Cd_{0.23}Te$,[5] implying that spin-polarized photocarriers themselves give magnetization below our detection limit. Beside, a high chop rate between left and right circular polarizations (37 kHz) precludes the appearance of

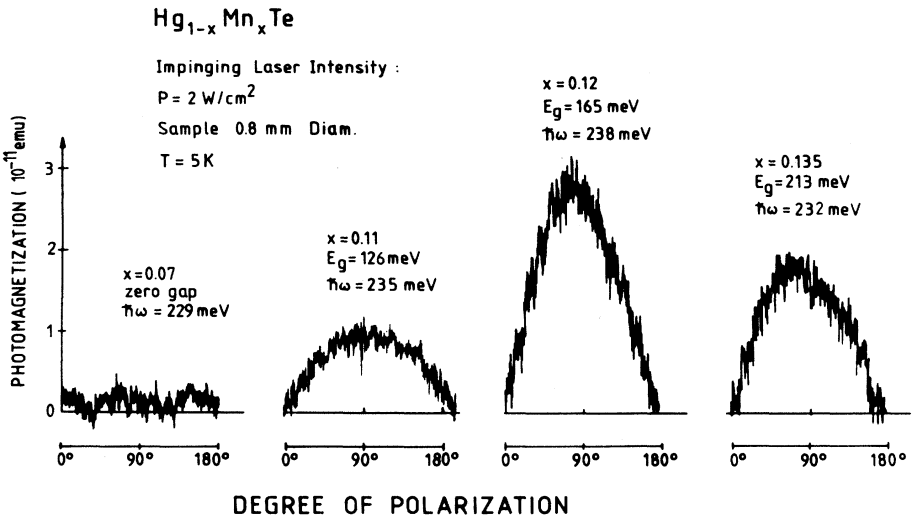

FIG. 3. Proof of "direct" photomagnetism in samples of $Hg_{1-x}Mn_xTe$; note the absence of any signal in the zero-gap sample $x=0.07$. The photomagnetization vanishes for linearly polarized excitation (0°, 180°) and has a maximum for circularly polarized excitation (90°). The vertical scale gives the total magnetic moment induced in the samples.

a significant polarization of nuclear spins (visible in nonmagnetic materials for time-independent circular polarization[9,12,21]). We thus conclude that the photomagnetization in question must originate from Mn d spins oriented by spin-polarized photocarriers. The maximum detected flux was about $(1\times10^{-3})\Phi_0$ for a laser-power of density 2 W/cm^2. Since the diffusion length of photoelectrons is about 10 μm in narrow-gap $Hg_{1-x}Mn_xTe$, this flux corresponds to a bulk magnetic moment of $\approx3.0\times10^{-11}$ emu in the volume $\approx5\times10^{-6}$ cm^3. Such magnetization ($\approx6\times10^{-6}$ emu/cm^3) would be produced by an external field of $\approx3\times10^{-2}$ Oe. A small value of the induced magnetization implies, in particular, that a feedback influence of polarized Mn spins on effective-mass electrons can be neglected. (The case of an extremely high excitation requiring inclusion of the feedback effects has been treated theoretically by Warnock and Awschalom.[22]) The temperature dependence of the induced magnetization for the $x=0.12$ sample is shown in Fig. 4. For this temperature range a $1/T$ dependence is observed. For comparison in Fig. 5 the dc susceptibility versus $1/T$ as determined by Nagata *et al.*[23] for a sample with $x=0.11$ is plotted together with results of a fit,

$$\chi_m(T)=\frac{c_m}{T-\Theta}+\chi_0 ,$$

in this small temperature range ($c_m=27.6\times10^{-5}$ emu K/g, $\Theta=-3.5$ K, $\chi_0=0.98\times10^{-5}$ g). Clearly, the optically induced magnetization and the susceptibility follow a similar, but not identical, temperature dependence. In our experimental setup the temperature of the sample is varied by changing the laser power from 2 to about 60 mW. Since the sample is situated either in liquid helium ($T=4.2$ K) or in exchange He gas, the absorbed laser power changes its temperature. As shown in Fig. 6, the photomagnetization first increases linearly with laser power. However, when increasing laser power further, the sample temperature increases and simultaneously the induced photomagnetization deviates considerably from a linear behavior. The temperature values indicated by the arrows in Fig. 6, as well as those in Fig. 4, were obtained by calibrating a temperature sensor at the position of the sample against a second one. All data shown in the Fig. 3 were obtained at laser powers of 10 mW, in the linear regime, which was also used for the observation of the wavelength dependence of the photomagnetization as described below.

Apart from the temperature dependence of the induced magnetization the response to the variation of the incident photon energy is also of importance for a physical understanding of the effect.[24,25] Unfortunately the use of

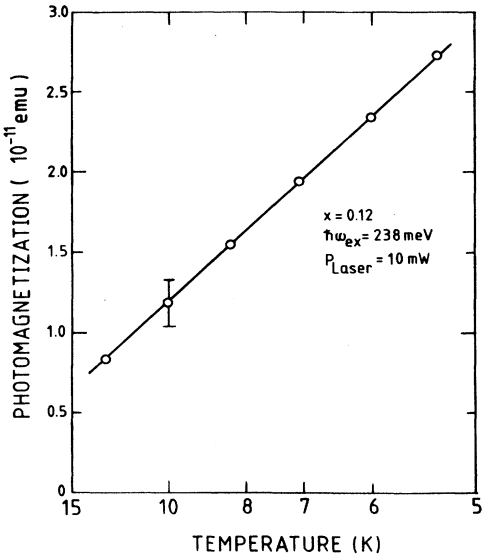

FIG. 4. Temperature dependence of the photomagnetization normalized to 10 W impinging laser power for $Hg_{1-x}Mn_xTe$ ($x=0.12$). Note the $1/T$ scale of the abscissa.

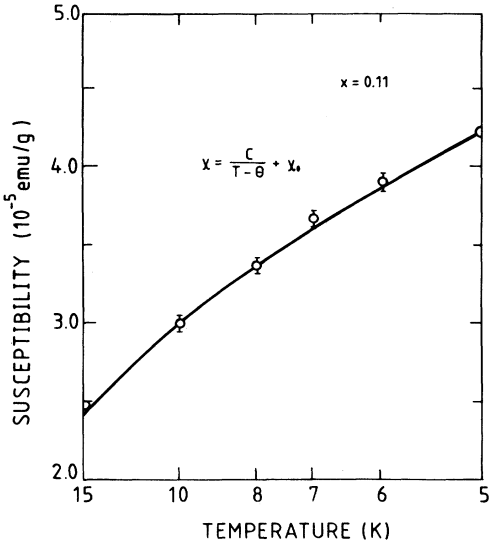

FIG. 5. Low-field susceptibility for $Hg_{1-x}Mn_xTe$ ($x=0.11$) as a function of temperature. The same scale ($1/T$) as in Fig. 4 is used. The solid line is a fit according to the Curie-Weiss formula with parameters C, Θ, and χ_0 given in the text. The data were taken from Ref. 23.

a CO laser limits the useful photon-energy range to 220–245 meV. The magnetization spectrum as a function of $\hbar\omega_{ex}$ is displayed for two samples in Figs. 7 and 8. There are distinct changes of the magnetization signal as the exciting laser frequency varies. In Fig. 7 ($x=0.135$) a relatively small induced flux at energies up to 228 meV is followed by a strong increase beyond the LO-phonon energy of the HgTe-like phonon of $Hg_{1-x}Mn_xTe$ ($\hbar\omega_{LO}=17$ meV). For still higher energies the observed signal decreases again. For this particular sample the experiment scans electron energies from below the LO energy to energies of about $2\hbar\omega_{LO}$, as depicted in Fig. 7. For a sample with a much smaller gap, Fig. 8, $x=0.11$, the induced magnetization is in its maximum about a factor of 2 smaller in the same energy range. As a consequence the signal-to-noise ratio decreases; note the increase of the error bars in Fig. 8. Each of the dots represents an average over ten individual measurements. The relatively small energy range ensures that the quantum efficiency for excitation is really constant. Thus the observed structures are an important clue to intrinsic relaxation phenomena.

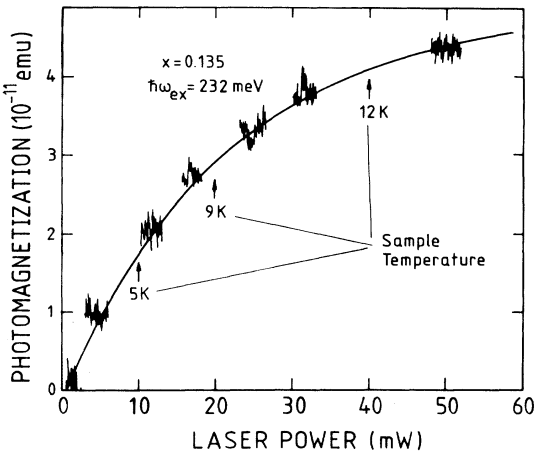

FIG. 6. The dependence of photomagnetization in $Hg_{1-x}Mn_xTe$ ($x=0.135$) on the impinging laser power. A linear relationship is observed only in the range up to 15 mW, below which most of the photomagnetization experiments were performed. For higher laser powers the sample temperature increases and the signal deviates from proportionality.

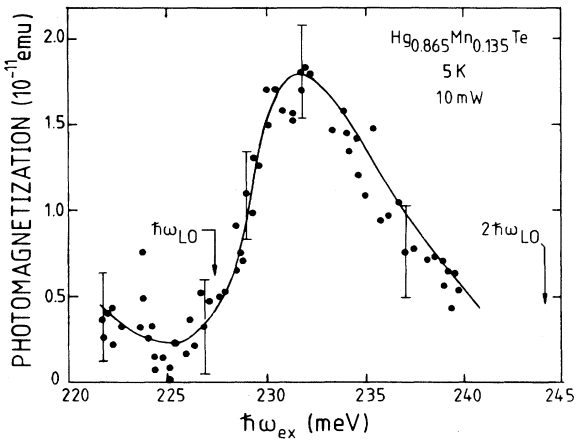

FIG. 7. Light-induced total magnetic moment vs exciting photon energy for $Hg_{1-x}Mn_xTe$ ($x=0.135$). Each dot is an average over ten individual measurements. The error bars indicate the maximum spread of experimental data, corresponding to a noise signal. The energetic distance of the minima coincides with the LO-phonon energy 17 meV.

Figures 7 and 8 imply that the emission of LO phonons by electrons excited sufficiently above the bottom of the conduction band is of crucial importance for the total magnetization signal. For excitations considerably above the conduction-band edge, as for the sample shown in

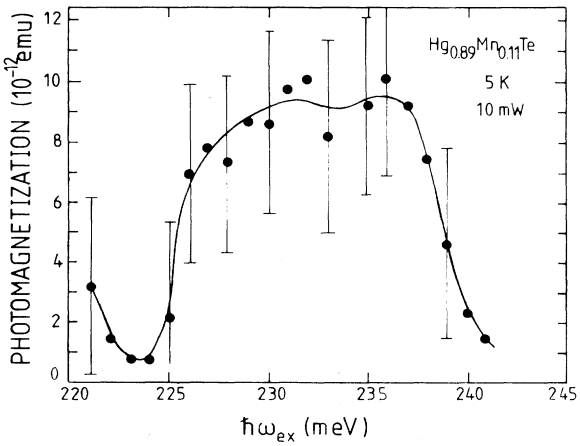

FIG. 8. Light-induced total magnetic moment vs exciting photon energy for $Hg_{1-x}Mn_xTe$ ($x=0.11$).

Fig. 8, a phonon-cascade process[26] will relax the energy, momentum, and spin of the nonequilibrium carriers and thus diminish their ability to order ferromagnetically the spins of the 3*d* Mn ions. These results also demonstrate that spin-polarized electrons, not holes, cause orientation of Mn spins. This is because in the case of holes no dependence on laser energy would be observed in this energy range due to the small curvature of the heavy-hole band.

IV. THEORY

A. Initial polarization

As sketched in Fig. 9, circularly polarized light produces two δ-like distributions of spin-polarized electrons, one originating from transitions from the heavy-hole (hh) band, the second from the light-hole (lh) band. The corresponding generation rates are described by the initial polarizations $P_i(\mathrm{hh}),P_i(\mathrm{lh})$ weighted by the joint density of states $(D_{\mathrm{hh}},D_{\mathrm{lh}})$ and by the transition probability matrix elements $(M_{\mathrm{hh}},M_{\mathrm{lh}})$:

$$(G_+-G_-)_{\mathrm{hh}}=\frac{P_i(\mathrm{hh})|M_{\mathrm{hh}}|^2D_{\mathrm{hh}}}{|M_{\mathrm{hh}}|^2D_{\mathrm{hh}}+|M_{\mathrm{lh}}|^2D_{\mathrm{lh}}}G\ , \tag{1}$$

$$(G_+-G_-)_{\mathrm{lh}}=\frac{P_i(\mathrm{lh})|M_{\mathrm{lh}}|^2D_{\mathrm{lh}}}{|M_{\mathrm{hh}}|^2D_{\mathrm{hh}}+|M_{\mathrm{lh}}|^2D_{\mathrm{lh}}}G\ , \tag{2}$$

where for σ^+ polarization

$$P_i=-\frac{n_+-n_-}{n_++n_-}\ , \tag{3}$$

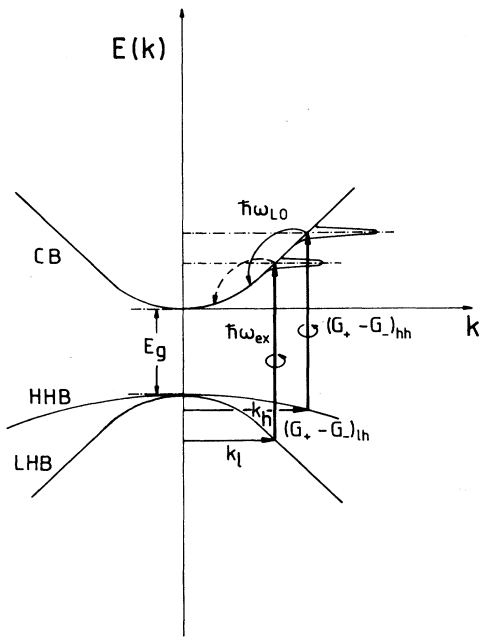

FIG. 9. Electrons injected from the heavy- and light-hole bands are rapidly transferred to the vicinity of the conduction-band bottom by optical-phonon emission. $(G_+-G_-)_{\mathrm{hh}}$ and $(G_+-G_-)_{\mathrm{lh}}$ are the generation rates of spin-polarized electrons in the conduction band.

and n_+,n_- denote the concentration of electrons oriented parallel and antiparallel to the propagation direction of light.

In the above formula G is the total generation rate per unit volume, which may be related to the impinging laser power P_L according to

$$\int d^3rG(\mathbf{r})=\frac{P_L(1-R-T)}{\hbar\omega_{\mathrm{ex}}}\ ,$$

where R is the reflectivity, T the transmission, and $\hbar\omega_{\mathrm{ex}}$ the laser photon energy. Because of nonparabolicity of the conduction and light-hole bands, corresponding expressions for $(G_+-G_-)_{\mathrm{hh,lh}}$ are rather complicated. The expressions for the transition matrix elements, the joint densities of states, and the initial spin polarizations for transitions from both bands (hh,lh) are given in Appendix A and can be readily expressed by band-structure parameters. The explicit values of material parameters that we will use in our calculations are displayed in Table I and Fig. 10. The value of the generation rate depends on E_g and the ratio E_g/Δ, as shown in Fig. 10. For $Hg_{1-x}Mn_xTe$, for the composition range of interest, $\Delta=1.08$ eV can be taken as constant. The energy gap of $Cd_{1-x}Mn_xTe$ ($x=0.2$) is 1.925 eV for 4.2 K and $\Delta=0.9$ eV, and thus $E_g/\Delta=2.14$. Therefore, for wide- and narrow-gap materials the amount of the initial spin polarization is not identical if an excitation to finite k values is considered. It should be noted that if the dominant contribution comes from the carriers excited from the heavy-hole band, then the generation rate is simply given by[9,14]

$$(G_+-G_-)_{\mathrm{hh}}=-\tfrac{1}{2}G\ .$$

B. Relaxation mechanisms

The generation rate (G_+-G_-) determines the spin-oriented electron concentration (n_+-n_-) together with the relevant relaxation rates and the diffusion process:

$$\frac{\partial(n_+-n_-)}{\partial t}=G_+-G_--(n_+-n_-)\frac{1}{\tau}+D\Delta(n_+-n_-)\ , \tag{4}$$

Actually there are two equations, one for the generation from the heavy-hole band and one for the generation from the light-hole band. In the above equation D is the diffusion constant; the relaxation time τ takes into account energy- and spin-relaxation processes and may be written in the form

$$\frac{1}{\tau}=\frac{1}{\tau_{\mathrm{rec}}}+\frac{1}{T_{1e}}\ . \tag{5}$$

Here, τ_{rec} is the radiative and nonradiative lifetime, and T_{1e} incorporates all nonspin-conserving mechanisms. Under stationary conditions the solution of the above equation assumes a form

TABLE I. Parameters of narrow- and wide-gap semimagnetic semiconductors used for calculation of photomagnetization (at $T=4.2$–5 K).

Material	$Hg_{1-x}Mn_xTe$ $x=0.11$	$Hg_{1-x}Mn_xTe$ $x=0.12$	$Hg_{1-x}Mn_xTe$ $x=0.135$	$Cd_{1-x}Mn_xTe$ $x=0.2$
E_g (meV)	126	165	213	1925
Δ (meV)	1080	1080	1080	900
P (eV cm)	7.5×10^{-8}	7.3×10^{-8}	7.2×10^{-8}	9.7×10^{-8}
αN_0 (eV)	-0.4[a]	-0.4	-0.4[a]	-0.216[b]
βN_0 (eV)	0.6[a]	0.6	0.6[a]	0.84[b]
χ (emu/g)[b]	4×10^{-5}	4×10^{-5}	4×10^{-5}	9×10^{-5}
m_h/m_0	0.45	0.45	0.45	0.63
m_{cv}/m_0	1.32	1.32	1.32	1.32
$h\omega_{LO}$ (meV)	17	17	17	21
$1/\epsilon_\infty-1/\epsilon_s$	0.025	0.025	0.025	0.047
Sample diam (μm)	800	800	800	10[c]
P_L (mW)	10	10	10	5[c]
m_1 (emu)	9.4×10^{-12}	2.8×10^{-11}	1.8×10^{-11}	4.3×10^{-15}[c]

[a]Reference 48.
[b]Reference 1.
[c]References 7 and 8.

$$n_+-n_-=\frac{\alpha(1-R-T)P_LP_i}{A\hbar\omega_{ex}}\left[\frac{\tau}{D}\right]^{1/2}\frac{1}{\alpha^2-\frac{1}{\tau D}}\times\left[\alpha\exp\left[-\frac{z}{\sqrt{\tau D}}\right]-\frac{1}{\sqrt{\tau D}}\exp(-z\alpha)\right], \tag{6}$$

where A is the sample area, z is the distance from the surface and α is the absorption coefficient. The photomagnetization signal depends on total number of spin-polarized carriers, N_s, rather than on their density. Integrating n_+-n_- over z, one obtains

$$N_s=\frac{(1-R-T)P_LP_i\tau}{\hbar\omega_{ex}}. \tag{7}$$

Thus, as is expected N_s does not depend on the diffusion efficiency, and therefore in the following we shall omit the diffusion term.

Since the experimental data shown in Figs. 7 and 8 clearly indicate that the measured magnetization depends on $\hbar\omega_{ex}$ and exhibits structures associated with the LO-phonon energy of $Hg_{1-x}Mn_xTe$, we consider the following rate equations for the calculation of n_+-n_-, which takes into account inelastic phonon scattering:

$$\left.\frac{\partial(n_+-n_-)}{\partial t}\right|_{m\hbar\omega_{LO}}=G_+-G_--(n_+-n_-)|_{m\hbar\omega_{LO}}\left.\left[\frac{1}{\tau_{rec}}+\frac{1}{\tau_{po\uparrow\uparrow}}+\frac{1}{\tau_{po\downarrow\uparrow}}+\frac{1}{T_{1e}}\right]\right|_{m\hbar\omega_{LO}},$$

$$\left.\frac{\partial(n_+-n_-)}{\partial t}\right|_{(m-1)\hbar\omega_{LO}}=(n_+-n_-)\left.\left[\frac{1}{\tau_{po\uparrow\uparrow}}-\frac{1}{\tau_{po\downarrow\uparrow}}\right]\right|_{m\hbar\omega_{LO}}-(n_+-n_-)|_{(m-1)\hbar\omega_{LO}}\times\left.\left[\frac{1}{\tau_{rec}}+\frac{1}{\tau_{po\uparrow\uparrow}}+\frac{1}{\tau_{po\downarrow\uparrow}}+\frac{1}{T_{1e}}\right]\right|_{(m-1)\hbar\omega_{LO}}, \tag{8}$$

$$\left.\frac{\partial(n_+-n_-)}{\partial t}\right|_{0\times\hbar\omega_{LO}}=(n_+-n_-)\left.\left[\frac{1}{\tau_{po\uparrow\uparrow}}-\frac{1}{\tau_{po\uparrow\downarrow}}\right]\right|_{\hbar\omega_{LO}}-(n_+-n_-)|_{0\times\hbar\omega_{LO}}\left.\left[\frac{1}{\tau_{rec}}+\frac{1}{T_{1e}}\right]\right|_{0\times\hbar\omega_{LO}}.$$

The labeling of the energies is counted from the bottom of the conduction band in multiples m of $\hbar\omega_{LO}$ (i.e., the label 0 corresponds to an excitation below $\hbar\omega_{LO}$).

For stationary conditions Eqs. (8) are solved for the population of the energy level $E=n\hbar\omega_{LO}$ and $E'=n'\hbar\omega_{LO}$ due to excitations form the heavy- and light-hole bands, respectively. We write explicitly the solution for the former case:

$$(n_+-n_-)|_n=GP_i(\mathrm{hh})T_{\mathrm{hh}}|_n,$$

where

$$T_{\mathrm{hh}}|_n = \frac{\prod_{j=n+1}^{m} \left[\frac{1}{\tau_{po\uparrow\uparrow}} - \frac{1}{\tau_{po\uparrow\downarrow}} \right]_j}{\prod_{j=n}^{m} \left[\frac{1}{\tau_{\mathrm{rec}}} + \frac{1}{\tau_{po\uparrow\uparrow}} + \frac{1}{\tau_{po\uparrow\downarrow}} + \frac{1}{T_{1e}} \right]_j} ; \quad (9)$$

τ_{po} is either the spin-conserving ($\uparrow\uparrow$) or spin-flip ($\downarrow\uparrow$) relaxation time due to interaction with the polar-optical phonons.[27] Their explicit form is given in Appendix B. For the sake of simplicity, we neglect nonpolar electron-phonon coupling as well as the presence of MnTe-like LO-phonon modes.

Apart from polar-optical spin-flip scattering ($\tau_{po\downarrow\uparrow}$), we shall consider three kinds of other spin-relaxing phenomena: the Elliott-Yafet (T_{EY}) and D'yakonov-Perel' (T_{DP}) mechanisms, as well as spin exchange with Mn ions ($T_{e\mathrm{Mn}}$):

$$\frac{1}{T_{1e}} = \frac{1}{T_{\mathrm{EY}}} + \frac{1}{T_{\mathrm{DP}}} + \frac{1}{T_{e\mathrm{Mn}}} .$$

As is known, the Elliott-Yafet mechanism occurs due to the fact that the band structure is strongly affected by spin-orbit interaction and the wave functions of the conduction band contain p-type admixtures. Therefore, the spin ceases to be a good quantum number and all scattering mechanisms partly relax the initial spin polarization.[10,14,28] The corresponding spin-relaxation rates may be written in the form[10,14]

$$\frac{1}{T_{\mathrm{EY}}} \approx \frac{16}{27} \frac{1}{\tau_m} \left[\frac{E_c(k)}{E_g} \right]^2 \eta^2 \frac{1-\frac{1}{2}\eta}{1-\frac{1}{3}\eta} , \quad (10)$$

where

$$\eta = \frac{\Delta}{E_g + \Delta} ,$$

and τ_m is the momentum-relaxation time, excluding optical-phonon scattering, which is treated separately (it is described by $1/\tau_{po\uparrow\downarrow}$). We assume that τ_m does not depend on electron energy $E_c(k)$, a justifying approximation in the view that τ_m is presumably determined by scattering by neutral acceptors. It should be noted in this context that because of the p-type character of the valence band the Elliott-Yafet process if very efficient for holes. Because of that, holes lose their spin orientation very fast and their contribution to the orientation of the Mn ions can be neglected.

Due to the interaction with remote bands and due to the presence of spin-orbit interaction, the conduction band of the zinc-blende structure exhibits a k^3 splitting

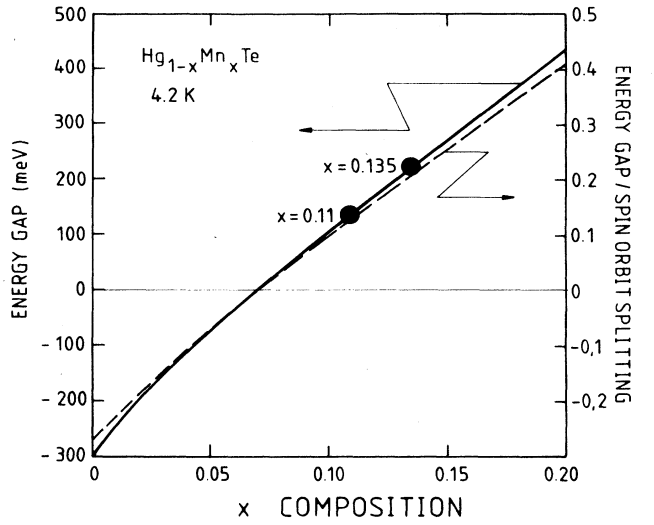

FIG. 10. Dependence of the energy gap on the fractional Mn concentration. The dots denote the location of the samples under investigation. On the right ordinate scale the relative importance of the energy gap and spin-orbit interaction is indicated, which influences the degree of initial spin polarization of excited carriers.

which is not included in the expressions given so far. D'yakonov and Perel'[29] have shown that the k^3 splitting can be treated as an effective relaxation mechanism for the spin orientation, provided this splitting is smaller than the inverse of the momentum-relaxation time. Under these conditions the D'yakonov-Perel' relaxation rate is[10,14]

$$\frac{1}{T_{\mathrm{DP}}} \approx 0.08\tau'_m \left[\frac{\Delta}{\hbar} \right]^2 \left[\frac{m^*(k)}{m_{cv}} \right]^2 \times \frac{1}{(1+\Delta/E_g)(1+2\Delta/E_g)} \left[\frac{E_c(k)}{E_g} \right]^3 , \quad (11)$$

where

$$\frac{1}{\tau'_m} = \frac{1}{\tau_m} + \frac{1}{\tau_{po\uparrow\uparrow}}$$

and $m(k)$ denotes the k-dependent effective mass in the conduction band and m_{cv} an interband mass characterizing the strength of interaction with the far bands.

The third mechanism which relaxes the spin of conduction electrons, and which is characteristic for magnetic materials is that which is caused by s-d-like interaction, $-J\mathbf{S}\cdot\mathbf{s}$. For the conduction electrons, we use the following expression:[30,31]

$$\frac{1}{T_{e\mathrm{Mn}}} = \frac{\chi k_B T k m^*(k)}{\pi\hbar^3 g^2 \mu_B^2} \left[a_c^4\alpha^2 + \frac{1}{4} \left[c_c^4 + \tfrac{5}{6} b_c^4 + \frac{2b_c^2 c_c^2}{3} + \frac{2\sqrt{2}}{3} b_c^3 c_c \right] \beta^2 \right] , \quad (12)$$

where

$$\alpha=\langle S|J|S\rangle,\ \beta=\langle X|J|X\rangle \tag{13}$$

are the s-d and p-d exchange integrals, χ is the magnetic susceptibility of Mn spins, and $g=2.0$ is their Landé factor; a_c, b_c, c_c describe s-type (a_c) and p-type (b_c, c_c) components in the Bloch function, given explicitly in Ref. 32.

In contrast to narrow-gap materials, in wide-gap materials one has to consider a further step in the thermalization process: Results of optical pumping[11] as well as those on photoconductivity in wide-gap materials[33] imply that the emission of phonons does not end up in the conduction band, but electrons are trapped in the picosecond time scale[34] by shallow donors. Under this condition the spin depolarization is no longer described by Eq. (12), but is determined by a fluctuating exchange field experienced by the hopping electrons.[11] The corresponding relaxation time is given by

$$\frac{1}{T_{e\mathrm{Mn}}}=\frac{4\Delta^2\tau_c}{3\hbar^2}\ , \tag{14a}$$

with

$$\Delta=(8E_p k_B T)^{1/2}\ , \tag{14b}$$

$$E_p=\frac{\alpha^2\chi}{32\pi a_B^3 g^2\mu_B^2}\ , \tag{14c}$$

where Δ is the most probable value of the spin splitting of donor levels in the absence of the magnetic polaron effect,[15] τ_c is the correlation time (of the order of the hopping time from one donor to another), and a_B is the Bohr radius. Formula (14a) is strictly valid under motional-narrowing conditions,[11] i.e., for $\tau_c<\hbar/(8E_p k_B T)^{1/2}$.

In Figs. 11–13 the calculated relaxation rates are shown as a function of the initial carrier energy in the conduction band for two $Hg_{1-x}Mn_xTe$ samples and a $Cd_{1-x}Mn_xTe$ sample. For the four important relaxation mechanisms, the value of E_g/Δ is the crucial quantity, along with the Fröhlich polar-phonon coupling parameter (also see Table I): For the two narrow-gap materials the relaxation rates $1/T_{e\mathrm{Mn}}$ are rather small as compared to that for $Cd_{0.8}Mn_{0.2}Te$. The relative importance of the spin-flip mechanisms due to the Elliott-Yafet and D'yakonov-Perel' relaxation also varies with E_g/Δ. For higher values of E_g/Δ the DP mechanism finally is the leading one. In the narrow-gap case, at lower energies the EY mechanism is the dominant spin-relaxation mechanism.

It is interesting to compare the relative importance of the spin-spin exchange rate between polarized free carriers and the Mn subsystem, $1/T_{e\mathrm{Mn}}$, with all the other non-spin-conserving mechanisms. In Fig. 14 a plot of $1/T_{e\mathrm{Mn}}$ divided by

$$\frac{1}{\tau_{po\downarrow\uparrow}}+\frac{1}{T_{\mathrm{DP}}}+\frac{1}{T_{\mathrm{EY}}}+\frac{1}{T_{e\mathrm{Mn}}}=\frac{1}{\tau_{po\downarrow\uparrow}}+\frac{1}{T_{1e}}$$

as a function of E_c is shown for various values of E_g/Δ. The momentum-relaxation rate $1/\tau_m=1\times10^{13}\ \mathrm{s}^{-1}$ was adopted for this calculation. It is clearly seen that the relative importance of $1/T_{e\mathrm{Mn}}$ increases with the energy gap or when the carrier energy approaches zero.

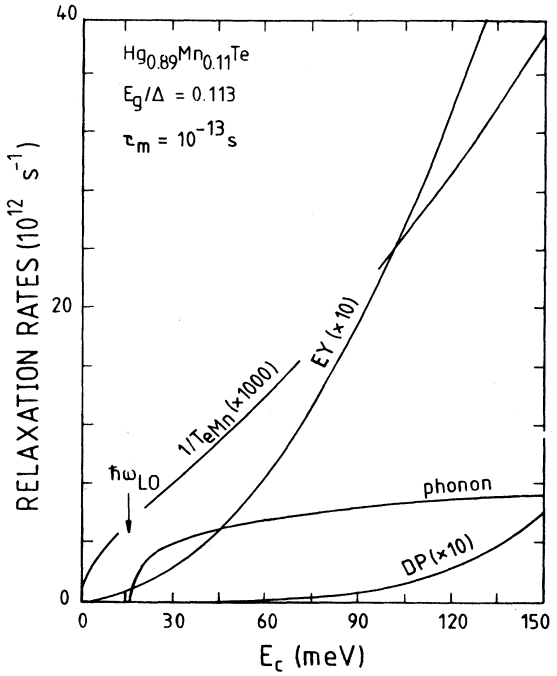

FIG. 11. Relaxation rates vs carrier energy for $Hg_{1-x}Mn_xTe$ ($x=0.11$). The polar-optical-phonon scattering is mainly spin conserving and transfers electrons to energies below the LO-phonon energy (17 meV). $T_{e\mathrm{Mn}}$ is the exchange-scattering time (electrons–Mn ions), whereas EY denotes the non-spin-conserving Elliott-Yafet mechanism, and DP is the D'yakonov-Perel' mechanism, which relaxes the carrier spin polarization most effectively at higher energies due to k^3 splitting in the noncentrosymmetric zinc-blende crystal. The momentum relaxation time was taken as $\tau_m=10^{-13}$ s.

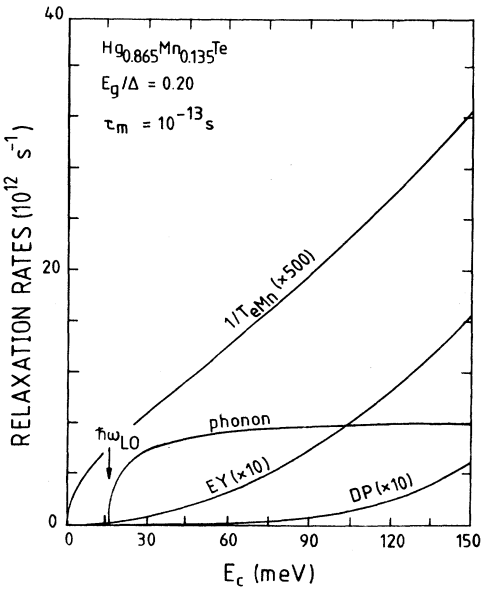

FIG. 12. Same as Fig. 11, for $Hg_{1-x}Mn_xTe$ ($x=0.135$). The EY mechanism is decreased with respect to Fig. 11, whereas the carrier–Mn-ion exchange scattering is twice as much for $x=0.11$.

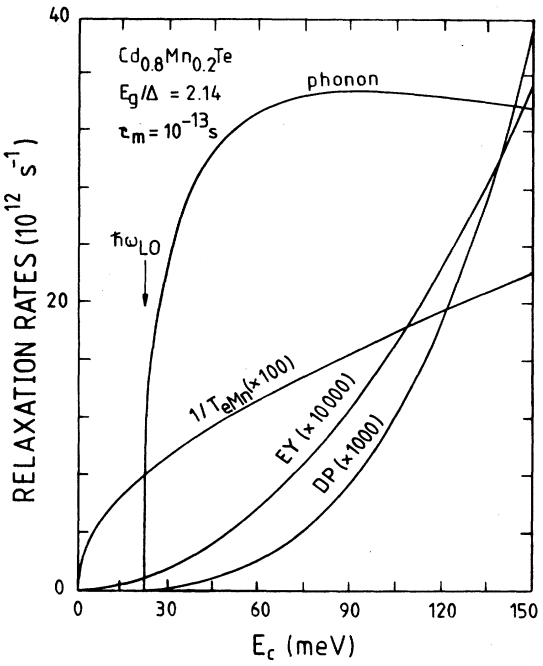

FIG. 13. Same as Fig. 11, for $Cd_{1-x}Mn_xTe$ ($x=0.2$). In this wide-gap semiconductor the polar-optical-phonon scattering and the carrier–Mn-ion exchange scattering are much more effective than in the narrow-gap material ($Hg_{1-x}Mn_xTe$). The EY mechanism can be neglected.

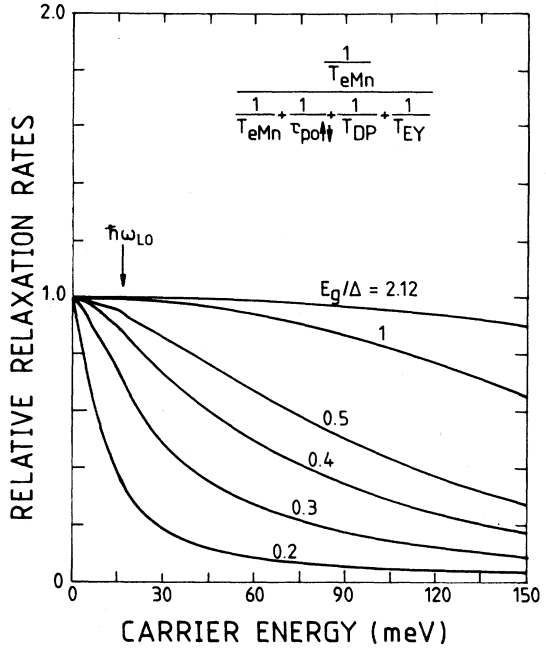

FIG. 14. Electron–Mn-ion exchange scattering rate, divided by the overall spin-flip relaxation rates, vs carrier energy. This ratio describes the effectiveness of the coupling between spin-polarized carriers and localized Mn ions. The momentum relaxation time of 10^{-13} s was taken for this calculation.

C. Exchange interaction: Mean-field mechanism and dynamical polarization

As discussed in the preceding sections, a circularly polarized light produces a stationary spin density of s electrons, $\frac{1}{2}(n_+ - n_-)$, oriented in the direction of the light propagation (z direction). Thus, under the presence of the exchange interaction, $-J\mathbf{S}\cdot\mathbf{s}$, the Mn spins experience a mean (molecular) field. This field is pointed along the z direction and is readily given by[35]

$$B^* = -\frac{n_+ - n_-}{2g\mu_B}\alpha \ , \tag{15}$$

where α is the s-d exchange integral defined by Eq. (13) and $g=2.0$ is the Landé factor of Mn spins. Since the chop rate between the left and right circular polarizations is surely smaller than the spin-lattice relaxation rate of Mn spins, this B^* can be regarded as a static magnetic field. Hence, it will induce a magnetization which may be written in the form

$$M_1 = \chi(T)B^* = -\chi(T)\frac{n_+ - n_-}{2g\mu_B}\alpha \ , \tag{16}$$

where $\chi(T)$ denotes the temperature-dependent static magnetic susceptibility of Mn ions. As seen from Eq. (16), the temperature dependence of M_1 is determined by that of χ, providing $n_+ - n_-$ is temperature independent. This takes place when the spin-relaxation time is dominated by mechanisms other than the s-d exchange interaction. However, if the latter mechanism is the leading one, one sees from Eqs. (9) and (12) that $T_{e\mathrm{Mn}}$ and hence $n_+ - n_-$ is inversely proportional to $\chi(T)T$. Thus, in this case M_1 becomes inversely proportional to T.

It is interesting to note that M_1 can be formally expressed by an effective Landé factor of electrons due to the s-d exchange interaction,[36]

$$\bar{g} = \frac{\alpha\chi}{g\mu_B^2} \ . \tag{17}$$

In terms of $\bar{g}$, M_1 becomes

$$M_1 = -\tfrac{1}{2}\bar{g}\mu_B(n_+ - n_-) \ . \tag{18}$$

For typical values of α and χ, $\bar{g}\simeq 10^2$ in semimagnetic semiconductors at low temperatures. Hence, we see immediately that the magnetization of Mn spins, M_1, is much larger than that of photoelectrons, $-\frac{1}{2}g\mu_B(n_+ - n_-)$, as $g\approx 2$ in the latter case (the magnetic moment of photoelectrons is not induced by a magnetic field and therefore neither spin-orbit nor s-d corrections to g appear). This, in particular, explains why in nonmagnetic narrow-gap materials with large effective g factors like InSb or $Cd_{1-x}Hg_xTe$ no photomagnetization was detected by us.[5]

In a previous report[5] on light-induced magnetization the second source for magnetization was considered, namely that which originates from the off-diagonal terms of the s-d interaction $\mathbf{s}_+\mathbf{S}_- + \mathbf{s}_-\mathbf{S}_+$. For a finite Mn-ion spin-lattice relaxation time $T_{\mathrm{Mn,ph}}$, and neglecting the spin-spin interaction between Mn ions, both the mean

field term and the spin-flip term (dynamic polarization) can be combined in a rate equation for the excess concentration of oriented Mn ions. For the sake of simplicity, we shall describe the Mn-spin polarization in terms of the occupation of just two levels with concentrations N_+ and N_-. By assuming that the equilibrium density $(N_+^0 - N_-^0)$ corresponds to that caused by the effective field B^*, one obtains

$$\frac{\partial(N_+ - N_-)}{\partial t} = 2N_- n_+ W_+ - 2N_+ n_- W_- - \frac{(N_+ - N_-) - (N_+^0 - N_-^0)}{T_{\mathrm{Mn,ph}}} . \tag{19}$$

The first two terms on the right-hand side of Eq. (19) correspond to the off-diagonal contribution (dynamic polarization). The terms W_+ and W_- are the spin-flip rates between the two subsystems, and their ratio is given by

$$\frac{W_+}{W_-} = \exp\left[-\frac{\hbar\omega_s - \hbar\omega_j}{k_B T} \right] . \tag{20}$$

$\hbar\omega_s$ and $\hbar\omega_j$ are, respectively, the energy splittings of the electrons ($\hbar\omega_s$) and Mn ions ($\hbar\omega_j$) in the molecular and external fields. For the stationary case, Eq. (19) yields a solution for $N_+ - N_-$:

$$N_+ - N_- = \frac{(N_+^0 - N_-^0) T_{\mathrm{Mne}}}{T_{\mathrm{Mn,ph}} + T_{\mathrm{Mne}}} + \frac{(N_+^0 + N_-^0)(n_+ W_+ - n_- W_-)}{\frac{1}{T_{\mathrm{Mn,ph}}} + \frac{1}{T_{\mathrm{Mne}}}} , \tag{21}$$

where

$$\frac{1}{T_{\mathrm{Mne}}} = n_+ W_+ + n_- W_- . \tag{22}$$

$T_{\mathrm{Mn,ph}}$ represents the spin relaxation of the Mn spins due to several mechanisms such as phonon scattering, hyperfine interaction with the nucleus, and scattering by the photoexcited holes in the valence band as well as by the bound holes.

If we assume that $1/T_{\mathrm{Mn,ph}} \gg 1/T_{\mathrm{Mne}}$, one obtains $(N = N_+ + N_-)$

$$N_+ - N_- = N_+^0 - N_-^0 + N T_{\mathrm{Mn,ph}} (n_+ W_+ - n_- W_-) . \tag{23}$$

Since under our experimental conditions $W_+ \approx W_-$, we obtain

$$N_+ - N_- \simeq N_+^0 - N_-^0 + N \frac{T_{\mathrm{Mn,ph}}}{T_{\mathrm{Mne}}} \frac{n_+ - n_-}{n_+ + n_-} . \tag{24}$$

If, however,

$$\frac{1}{T_{\mathrm{Mne}}} \gg \frac{1}{T_{\mathrm{Mn,ph}}}$$

(which means that the spins of the Mn ions are coupled strongly to the reservoir provided by the electron spins), we get

$$N_+ - N_- \simeq N T_{\mathrm{Mne}} (n_+ W_+ - n_- W_-) \approx N \frac{n_+ - n_-}{n_+ + n_-} . \tag{25}$$

In order to estimate T_{Mne}, we take $T_{e\mathrm{Mn}} = 10^{-12}$ s for the spin-spin exchange scattering time of electrons by Mn spins. Using the relation between T_{Mne} and $T_{e\mathrm{Mn}}$, we then get

$$T_{\mathrm{Mne}} \approx T_{e\mathrm{Mn}} \frac{N}{n_+ + n_-} \approx 10^{-2} \text{ s} .$$

Thus, for $N \approx 10^{22}$ cm^{-3} and $n_+ + n_- \approx 10^{12}$ cm^{-3}, the inequality $1/T_{\mathrm{Mn,ph}} \gg 1/T_{\mathrm{Mne}}$ indeed holds. Therefore, in this approximation [see Eq. (24)] the total magnetization of the Mn ions is produced by two parts, M_1 and M_2. Apart from the first (mean-field) term produced by the molecular field B^*, there is a second term, M_2, which comes from the off-diagonal part of the *s-d* exchange Hamiltonian (dynamic polarization):

$$M = M_1 + M_2 = -\chi(T) \frac{n_+ - n_-}{2 g \mu_B} \alpha - \frac{g \mu_B T_{\mathrm{Mn,ph}}}{2 T_{e\mathrm{Mn}}} (n_+ - n_-) , \tag{26}$$

where $T_{e\mathrm{Mn}}$ is given in Eq. (12). The above relation is valid for an arbitrary value of total Mn spin S (Ref. 37).

In order to estimate the relative importance of both terms M_1 and M_2, it is necessary to consider the influence of spin-spin interactions on the polarization of Mn spins. In the case of the static polarization M_1, these interactions are included by taking experimental values of $\chi(T)$. The case of the dynamic polarization is more involved and can be best analyzed in the framework of the spin-temperature theory.[12] According to that theory we divide the total Hamiltonian of the Mn-spin subsystem into three parts. The first of them is the Zeeman contribution:

$$\mathcal{H} = g \mu_B \sum_i \mathbf{B} \cdot \mathbf{S}_i , \tag{27}$$

where $\mathbf{B}$ is a sum of an external and molecular field $\mathbf{B}^*$. The second part includes those components of spin-spin interactions that can be described by the Heisenberg Hamiltonian,

$$\mathcal{H}_s = -\sum_{i,j} J_{ij} \mathbf{S}_i \cdot \mathbf{S}_j . \tag{28}$$

Finally, the third part, $\mathcal{H}_{\mathrm{ns}}$, takes into account nonscalar couplings which can come from the dipole, pseudodipole, and Dzyaloshinskii-Morija interaction. It is convenient to introduce local magnetic fields corresponding to $\mathcal{H}_s$ and $\mathcal{H}_{\mathrm{ns}}$:

$$B_{s(\mathrm{ns})}^2 = \frac{3 \mathrm{Tr} \mathcal{H}_{s(\mathrm{ns})}^2}{g^2 \mu_B^2 \sum_i \mathrm{Tr} S_i^2} . \tag{29}$$

In terms of these local magnetic fields, M_2 assumes the

form[12]

$$M_2=-\frac{g\mu_B T_1^*}{2T_{e\mathrm{Mn}}}(n_+-n_-)\ , \tag{30}$$

where

$$T_1^*=\frac{B^2}{\frac{1}{T_{\mathrm{Mn,ph}}}B^2+\frac{1}{T_s}B_s^2+\frac{1}{T_{\mathrm{ns}}}B_{\mathrm{ns}}^2}\ . \tag{31}$$

Here, $T_{\mathrm{Mn,ph}}$, T_s, and T_{ns} are relaxation times of energy corresponding to the Zeeman, scalar, and nonscalar interactions, respectively. The physical interpretation of the above formula is as follows: The magnetization M_2 is inversely proportional to the spin temperature. The spin temperature can be decreased by dynamic polarization to an extent determined by the heat capacitance of various reservoirs (proportional to B^2, B_S^2, and B_{ns}^2, respectively, and their energy-relaxation rates $1/T_{\mathrm{Mn,ph}}$, $1/T_s$, and $1/T_{\mathrm{ns}}$). Since the fast energy relaxation proceeds presumably through Mn clusters,[7,38,39] while Zeeman's energy comes mostly from isolated Mn spins, one may expect

$$T_{\mathrm{Mn,ph}}>T_s,T_{\mathrm{ns}}\ . \tag{32}$$

An upper limit of T_1^* can be thus estimated from

$$T_1^*=T_{\mathrm{Mn,ph}}\frac{B^2}{B^2+B_{\mathrm{ns}}^2}\ . \tag{33}$$

It is well known that the local magnetic field B_{ns} is a quantity which can be derived from EPR experiments. It is related to the second moment of the EPR line, which is simply proportional to the square of its half-width, $(\Delta H)^2$. The measured width of the EPR line[40–42] implies that $\Delta H\approx B_{ns}\geq 1$ kG for our Mn concentrations. Since in the case under consideration B is of the order of the Earth's magnetic field, we see that spin precession induced by local fields reduces M_2 by more than 6 orders of magnitude. Taking 10^{-6} s as an upper bound for $T_{\mathrm{Mn,ph}}$ at $T\geq 4.2$ K, $x\geq 0.1$ (Ref. 39), we find $M_2/M_1\ll 10^{-2}$ for narrow-gap $Hg_{1-x}Mn_xTe$. We conclude that the detected photomagnetization was primarily caused by the mean-field effect. An observation of a sizable dynamic polarization would require more diluted materials, lower temperatures, or higher magnetic fields along the light direction.

V. COMPARISON BETWEEN EXPERIMENTAL RESULTS AND THEORETICAL CALCULATIONS

In order to compare the observed magnetization with a calculated one, we recall that the experiment provides the total magnetic moment m induced in the sample:

$$m=\int d\mathbf{r}\,M(\mathbf{r})\ . \tag{34}$$

Summarizing results of the preceding sections, we get for the mean-field part of the induced magnetic moment by electrons excited from the heavy- and light-hole bands:

$$m_1=-\frac{\alpha\chi(T)}{2g\mu_B}G_{\mathrm{tot}}\left[P_i(\mathrm{hh})\sum_{n=0}^{m}T_{\mathrm{hh}}|_n+P_i(\mathrm{lh})\sum_{n'=0}^{m'}T_{\mathrm{lh}}|_{n'}\right]\ , \tag{35}$$

where

$$G_{\mathrm{tot}}=\frac{P_L(1-R-T)}{\hbar\omega_{\mathrm{ex}}} \tag{36}$$

is the total number of photons absorbed per time unit.

Similarly, for the dynamic polarization we have

$$m_2=-\frac{g\mu_B T_1^*}{2}G_{\mathrm{tot}}\left[P_i(\mathrm{hh})\sum_{n=0}^{m}\frac{T_{\mathrm{hh}}}{T_{e\mathrm{Mn}}}\bigg|_n+P_i(\mathrm{lh})\sum_{n'=0}^{m'}\frac{T_{\mathrm{lh}}}{T_{e\mathrm{Mn}}}\bigg|_{n'}\right]\ . \tag{37}$$

According to the above model and numerical results presented in Figs. 11–13, electrons excited to the energy E_c above the bottom of the conduction band are rapidly scattered by optical phonons to the energy $E=E_c-n\hbar\omega_{\mathrm{LO}}$ in between $E=0$ and $E=\hbar\omega_{\mathrm{LO}}$. Therefore, a stationary value of the spin density and thus of the photomagnetization are primarily determined by spin lifetime of electrons in the energy range $0<E\leq\hbar\omega_{\mathrm{LO}}$. Besides, if scattering of electrons by Mn ions is the dominant mechanism which limits the spin lifetime of photoelectrons (i.e., $T_{\mathrm{hh}}\approx T_{e\mathrm{Mn}}$), and when excitations from the light-hole band can be neglected [i.e., $P_i(\mathrm{hh})\approx -0.5$ and $P_i(\mathrm{lh})\approx 0$], m_1 and m_2 assume a particularly transparent form,

$$m_1=\tfrac{1}{4}\bar{g}\mu_B G_{\mathrm{tot}}T_{e\mathrm{Mn}}(E)\ , \tag{38}$$

where $\bar{g}=\bar{g}(T)$ is the electron effective Landé factor due to the s-d exchange interaction, and

$$m_2=\tfrac{1}{4}g\mu_B G_{\mathrm{tot}}T_1^*\ , \tag{39}$$

where $g=2.0$ and T_1^* is the Mn-spin-lattice relaxation time corrected for local-field effects, as given in Eq. (23). Equations (38) and (39) constitute convenient formulas for estimates of the upper limit of m_1 and m_2, respectively.

As a first step in a quantitative comparison between measured and calculated photomagnetization in $Hg_{1-x}Mn_xTe$, we assume that the spin lifetime is limited by scattering of optical phonons and magnetic ions, i.e., we set $1/\tau_{\mathrm{rec}}=1/T_{EY}=1/T_{\mathrm{DP}}=0$. The theoretical values of photomagnetization signal as a function of excitation energy lead one to assume that at maximum the values are plotted in Fig. 15 for the mean-field model in comparison to the experimental data. We see that for the samples with the largest energy gap E_g the theoretical values are close to those observed experimentally, whereas the decrease of photomagnetization for small x is due to $1/\tau_{po\downarrow\uparrow}$. Moreover, since in the case under consideration $m_1\propto\chi(T)T_{e\mathrm{Mn}}$, where according to Eq. (12) $1/T_{e\mathrm{Mn}}\propto\chi(T)T$, the photomagnetization should be inversely proportional to temperature. Experimental data

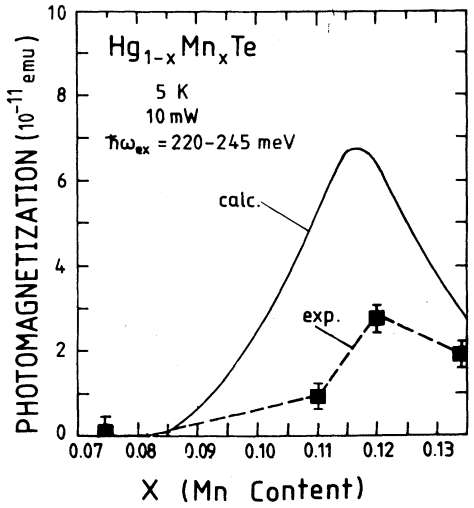

FIG. 15. Light-induced total magnetic moment vs composition x in $Hg_{1-x}Mn_xTe$ for photon energies of 220–245 meV, which give the maximum signal. Squares are experimental results; the solid line is calculated according to the mean-field model assuming that the spin lifetime of photoelectrons is limited by optical-phonon and exchange scattering of Mn ions, i.e., neglecting recombination as well as spin depolarization by the Elliott-Yafet and D'yakonov-Perel' mechanisms.

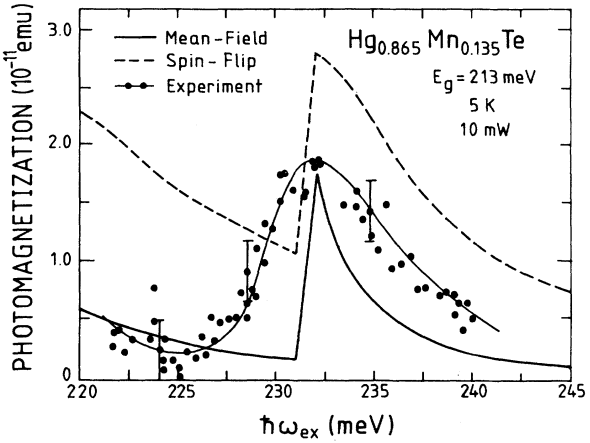

FIG. 16. Comparison of the mean-field (solid line) and the spin-flip (dashed line) calculated total light-induced magnetic moment with measured data (dots) for $Hg_{1-x}Mn_xTe$ ($x=0.135$) vs photon energy.

depicted in Fig. 4 follow this expectation.

With decreasing energy gap, the measured and calculated photomagnetization goes through a maximum, but the experimental values lie below the theoretical curve. We ascribe a low value of the measured photomagnetization in samples with the smallest E_g to the influence of additional shortening of spin life, which should be especially efficient in the narrow-gap case: the Elliott-Yafet process and possibly the Auger recombination. The comparison between measured and calculated photomagnetization, assuming finite values of T_{EY}, T_{DP}, and τ_{rec}, is shown in Figs. 16 and 17. The value of the momentum-relaxation time was fixed at $\tau_m=0.1$ ps, while τ_{rec} was treated as an adjustable parameter for each sample. This fitting procedure leads to $\tau_{rec}=5$ and 2 ns for $x=0.135$ and 0.11, respectively. It is not astonishing that the calculated energy dependence of magnetization is sharper than that determined experimentally, as no randomization of initial δ-like carrier distribution by, e.g., acoustic phonons and interelectronic interaction was taken into account. The latter should be particularly important in the case of the narrowest-gap sample (Fig. 17), where the excitation energy is much larger than E_g.

For comparison, we also computed the photomagnetization brought about by the dynamic polarization, regarding T_1^* as an additional fitting parameter. The values of $T_1^*=46$ and 100 ns for $x=0.135$ and 0.11, respectively, deduced in this way seem to be unrealistically long if local field effects are taken into consideration along the lines presented in Sec. IV.

We now turn to the photomagnetization results of Awschalom *et al.*[7] for $Cd_{0.8}Mn_{0.2}Te$. We shall analyze these data under the assumption that nuclear effects are absent in spite of the presence of a nonzero time-averaged circular polarization. For the laser power of 5 mW and $\hbar\omega_{ex}>E_g$, $m\approx 4.10^{-15}$ emu was detected in Ref. 7. This number per one absorbed photon is about 10^3 times smaller than that observed by us in $Hg_{0.88}Mn_{0.12}Te$. This points to the existence of a very fast spin relaxation of photoelectrons in $Cd_{1-x}Mn_xTe$. As already mentioned, in the case of wide-gap materials one expects an efficient trapping of electrons by localized states near the conduction-band edge. Since the capture occurs within a very short time compared to the spin-flip time of conduction-band electrons, the photomagnetization is given by Eqs. (38) and (39) with $T_{e\mathrm{Mn}}$ determined by hopping processes, as given in Eq. (14). Since irrespective of excitation energy the spin relaxation occurs in the donor

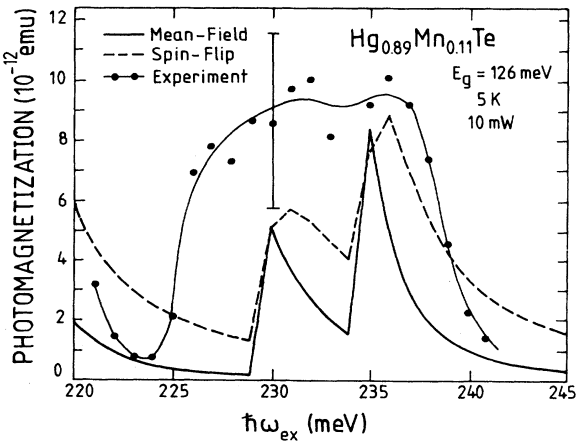

FIG. 17. Dependence of the total light-induced magnetic moment on the photon energy as measured (dots) and calculated according to spin-flip (dashed line) and mean-field (solid line) models for $Hg_{1-x}Mn_xTe$ ($x=0.11$).

states, no dependence of photomagnetization on $\hbar\omega_{ex}$ is expected for $\hbar\omega_{ex} > E_g$. This is in agreement with the experimental results. Moreover, under the assumption that the mean-field effect dominates, the data imply $T_{e\mathrm{Mn}} \approx 1.5$ ps, i.e., for $a_B = 50$ Å, $\tau_c \approx 1.3$ ps. The latter is close to the value deduced by Gaj[43] from optical pumping experiments in $Cd_{0.99}Mn_{0.01}Te$, $\tau_c = 7$ ps. It is worth noting that the fast spin relaxation induced by the *s-d* coupling also leads to a drastic reduction in the degree of luminescence polarization in $Cd_{1-x}Mn_xTe$,[42,43] as in the degree of luminescence polarization in $Cd_{1-x}Mn_xTe$ (Refs. 43 and 44) as compared to nonmagnetic materials.

It is also probable that the actual value of $T_{e\mathrm{Mn}}$ is even shorter than the estimate above, i.e., that the photomagnetization is caused, at least partially, by the dynamic polarization. Assuming that Eq. (39) also holds for localized electrons, the data imply $T_1^* \leq 70$ ps under the experimental conditions of Ref. 7.

As far as the increase of the photomagnetization signal below the band-gap excitation discovered by Awschalom *et al.*[7] is concerned, it is interesting to note that a strong increase of the degree of luminescence polarization in the same energy range has been observed by Warnock *et al.*[44] in optical pumping experiments on $Cd_{1-x}Mn_xTe$ and $Cd_{1-x}Mn_xSe$. These findings have been described[44] as being caused by creation of photoholes in the region where local magnetization has the right direction with respect to the hole spin. This may lead to a decrease of the hole spin relaxation and results in large value of both photomagnetization and degree of circular luminescence polarization.

VI. DISCUSSION AND CONCLUSIONS

The photoinduced magnetization in a dilute magnetic semiconductor is a valuable tool for studying relaxation phenomena. The effect originates in narrow-gap materials from the orientation of the Mn ions in the effective field of spin-polarized electrons. As far as the orientation of Mn ions via spin-flip scattering caused by the off-diagonal elements of the exchange Hamiltonian is concerned, the spin-spin interactions decrease substantially, by orders of magnitude, the contribution from the dynamic polarization to the total magnetization. Only for extremely diluted magnetic semiconductors could the orientation of the Mn ions by the spin-flip mechanism contribute considerably to the total magnetization.

In the analysis several assumptions were necessary. The spin orientation of the holes was neglected for $Hg_{1-x}Mn_xTe$ on the basis of their comparatively much shorter spin-relaxation time. In order to calculate the dependence of photomagnetization on photon energy, additional simplifying assumptions were made: for the initially injected δ-like distribution of hot spin-polarized electrons, no steady-state distribution function was derived using appropriate techniques. Instead, a simple model based on rate equations and cascade processes due to LO-phonon emission was considered using constant momentum-relaxation times. This rather crude approximation was used since the experimental results were obtained in a comparatively small photon-energy range, which is of the order of 20 meV. The main features, namely structures close to the LO-phonon mode energy in $Hg_{1-x}Mn_xTe$ and their absence in $Cd_{1-x}Mn_xTe$, are well accounted for. In $Hg_{1-x}Mn_xTe$ the relatively small absolute magnetization signal for injected electron energies below $E_g + \hbar\omega_{LO}$ is due to the importance of the spin-flip scattering events (Elliott-Yafet mechanism) caused by impurity and acoustic-phonon scattering, which diminish $n_+ - n_-$. This mechanism, which is particularly strong for narrow-gap materials, causes a steady decrease of $n_+ - n_-$ and thus of the magnetization with increasing carrier energy. However, for initial electron energies slightly above $\hbar\omega_{LO}$, the very effective Fröhlich interaction transfers excited electrons by LO-phonon emission towards the bottom of the conduction band, close to $k \approx 0$, where the Elliott-Yafet mechanism is rather ineffective and thus does not decrease effectively the initial electron polarization. For still higher initial energies, this transfer of carriers ends at electron energies and corresponding k values where the Elliott-Yafet mechanism is already important and thus the observed signal decreases again.

In the case of wide-gap $Cd_{1-x}Mn_xTe$ a relatively small value of photomagnetization was observed by Awschalom *et al.*[7] for $\hbar\omega_{ex} > E_g$. This, together with a small magnitude of luminescence polarization under optical pumping conditions,[43,44] implies the presence of very efficient spin relaxation. The fluctuating molecular field from Mn spins which comes about by trapped electrons hopping between donors can constitute the dominant effect in wide-gap materials. The corresponding scattering rate is inversely proportional to a_B^3, where a_B is the Bohr radius, which is comparatively small in these materials.

It should be stressed that the effect described is different from the so-called photomagnetization effects reviewed recently.[45] These authors deal with effects related to a change of the magnetization in ferromagnetic, antiferromagnetic, or at least spin-glass systems.

In conclusion, we point out that the polarization of the Mn spins in the photomagnetization experiments using circularly polarized band-gap radiation to inject spin-polarized carriers into the conduction band is caused by the molecular field of these carriers. The observed effect has both the correct order of magnitude, at least in $Hg_{1-x}Mn_xTe$, as well as the correct variation with temperature.

The second mechanism for the orientation of Mn ions, the dynamic polarization via the spin-flip scattering, is strongly reduced by interactions among the Mn ions.

In our paper we have focused on the photomagnetization in the limit of zero external magnetic field. In the high-field region, where the exchange splitting of bands becomes the dominating energy in the system, a number of novel phenomena related to photomagnetization can be also observed in dilute magnetic semiconductors.[46,47]

Note added in proof. The value for the photomagnetization given on p. 1513 of Ref. 5 differs by a factor of 20 from that given in this paper. This is due to uncertainties

in the previous determination of the magnetic coupling efficiency.

ACKNOWLEDGMENTS

The authors express their thanks to R. R. Gałazka and A. Mycielski for growing $Hg_{1-x}Mn_xTe$ samples. They are also very indebted to L. Swierkowski and W. Zawadzki for valuable discussions. This work was supported in part by the Fonds zur Förderung der wissenschaftlichen Forschung, Vienna, Austria, Project Nos. P 6476 P and P 5096.

APPENDIX A: JOINT DENSITY OF STATES, TRANSITION MATRIX ELEMENTS, AND INITIAL POLARIZATION IN NONPARABOLIC BANDS

According to Kane[32] the joint density of states for transitions from the valence bands j (heavy hole, hh; light hole, lh) to the conduction band (c) is given by

$$D_j=\frac{k^2}{2\pi^2|dE_c/dk-dE_j/dk|}\ . \tag{A1}$$

Expressing the dependence of D_j on k explicitly by the photon excitation energy $\hbar\omega_{\rm ex}$, the joint density of states for transitions from the light-hole band is given by

$$D_{\rm lh}(\hbar\omega_{\rm ex})=\frac{1}{\pi^2}\left[\frac{m_0^2}{2\hbar^2}\right]^{3/2}(E_g)^{1/2}\left[\frac{\hbar\omega_{\rm ex}}{E_g}\right]\left[\left[\frac{\hbar\omega_{\rm ex}}{E_g}\right]^2-1\right]^{1/2}, \tag{A2}$$

and, for the transition from the heavy-hole band,

$$D_{\rm hh}(\hbar\omega_{\rm ex})=\frac{\sqrt{2}}{\pi^2}\left[\frac{m_h}{\hbar^2}\right]^{3/2}\left\{\hbar\omega_{\rm ex}+\frac{E_g}{2}\left[\frac{m_h}{m_0^*}-1\right]-\frac{E_g}{2}\left[\left[\frac{m_h}{m_0^*}-1\right]^2+4\frac{m_h}{m_0^*}\frac{\hbar\omega_{\rm ex}}{E_g}\right]^{1/2}\right\}^{1/2}$$
$$\times\left[1-\frac{m_h/m_0^*}{[(m_h/m_0^*-1)^2+4(m_h/m_0^*)(\hbar\omega_{\rm ex}/E_g)]^{1/2}}\right], \tag{A3}$$

where m_0^* denotes the band-edge mass of the conduction band and m_h the heavy-hole mass.

The squares of the transition matrix elements for σ^+ radiation are given by

$$|M_{\rm lh}|^2=\tfrac{2}{3}P^2\{[a_c(k_l)b_l(k_l)+a_l(k_l)b_c(k_l)]^2+[a_c(k_l)c_l(k_l)-a_l(k_l)c_c(k_l)]^2\} \tag{A4}$$

and

$$|M_{\rm hh}|^2=\tfrac{2}{3}P^2a_c^2(k_h)\ , \tag{A5}$$

where $P=-i(\hbar/m_0)\langle S|p_z|Z\rangle$ is the momentum matrix element, and $a_i(k_j)$, $b_i(k_j)$, and $c_i(k_j)$ are the coefficients of the s- and p-type wave functions,[32] and k_j is the corresponding momentum wave-vector ($j=l,h$):

$$k_l=\left[\frac{m_0^*}{2\hbar^2}\right]^{1/2}\frac{1}{(E_g)^{1/2}}[(\hbar\omega_{\rm ex})^2-E_g^2]^{1/2} \tag{A6}$$

and

$$k_h=\left[\frac{2m_h}{\hbar^2}\right]^{1/2}(E_g)^{1/2}\left\{\frac{\hbar\omega_{\rm ex}}{E_g}+\frac{1}{2}\left[\frac{m_h}{m_0^*}-1\right]-\frac{1}{2}\left[\left[\frac{m_h}{m_0^*}-1\right]^2+4\frac{m_h}{m_0^*}\frac{\hbar\omega_{\rm ex}}{E_g}\right]^{1/2}\right\}^{1/2}. \tag{A7}$$

The initial polarization for a certain $\mathbf{k}$ direction is given by

$$P_i(\mathbf{k})=\frac{1}{|M_{\rm hh}|^2}\int\frac{d\phi\,d(\cos\theta)}{4\pi}(|\langle\tfrac{1}{2},\mathbf{k}|\mathcal{H}_I|\tfrac{3}{2},\mathbf{k}\rangle|^2+|\langle\tfrac{1}{2},\mathbf{k}|\mathcal{H}_I|-\tfrac{3}{2},\mathbf{k}\rangle|^2-|\langle-\tfrac{1}{2},\mathbf{k}|\mathcal{H}_I|\tfrac{3}{2},\mathbf{k}\rangle|^2-|\langle-\tfrac{1}{2},\mathbf{k}|\mathcal{H}_I|-\tfrac{3}{2},\mathbf{k}\rangle|^2), \tag{A8}$$

where

$$\mathcal{H}_I=\frac{\hbar^2}{m_0}(\nabla_x+i\nabla_y)$$

and

$$|M_{\rm hh}(\mathbf{k})|^2=\int\frac{d\phi\,d(\cos\theta)}{4\pi}(|\langle\tfrac{1}{2},\mathbf{k}|\mathcal{H}_I|\tfrac{3}{2},\mathbf{k}\rangle|^2+|\langle\tfrac{1}{2},\mathbf{k}|\mathcal{H}_I|-\tfrac{3}{2},\mathbf{k}\rangle|^2+|\langle-\tfrac{1}{2},\mathbf{k}|\mathcal{H}_I|-\tfrac{3}{2},\mathbf{k}\rangle|^2+|\langle-\tfrac{1}{2},\mathbf{k}|\mathcal{H}_I|-\tfrac{3}{2},\mathbf{k}\rangle|^2)\ . \tag{A9}$$

Replacing $(\frac{3}{2}|\mathbf{k})$ by $(\frac{1}{2}|\mathbf{k})$ and $(-\frac{3}{2}|\mathbf{k})$ by $(-\frac{1}{2}|\mathbf{k})$, one obtains the equations for the light-hole band (also see Fig. 9). The expressions for P_i(hh,lh) are finally given by

$$P_i(\mathrm{hh}) = -\tfrac{1}{2} , \tag{A10}$$

$$P_i(\mathrm{lh}) = -\tfrac{1}{2}\frac{2\sqrt{2}(a_c^2 b_l c_l - a_l^2 b_c c_c + a_l a_c b_c c_l - a_l a_c b_l c_c) - (a_c b_l + a_l b_c)^2}{(a_c b_l + a_l b_l)^2 + (a_c c_l - a_l c_c)^2} . \tag{A11}$$

APPENDIX B: SPIN-CONSERVING AND NON-SPIN-CONSERVING SCATTERING BY LO-PHONON EMISSION

The spin-conserving scattering is calculated to be starting with the expressions given in Refs. 27 and 28:

$$\frac{1}{\tau_{po\uparrow\uparrow}} = 2e^2\omega_{\mathrm{LO}}\left[\frac{1}{\epsilon_\infty}-\frac{1}{\epsilon_s}\right]\frac{[A+B(q_2-k)^2]^{1/2}}{Bk} \times\left\{\left[1-L\left[2-\frac{1}{2k}\frac{q_2^2}{q_2-k}\right]\right]^2\ln\left[\frac{q_2}{q_1}\right]-\frac{L}{2k}\left[1-L\left[2-\frac{1}{2k}\frac{q_2^2}{q_2-k}\right]\right]^2\frac{q_2^2-q_1^2}{q_2-k}+\frac{L^2}{16k^2}\frac{1}{q^2-k^2}(q_2^4-q_1^4)\right\} , \tag{B1}$$

where ϵ_∞ and ϵ_s denote the high-frequency and static dielectric constants, $A=(E_g/2)^2$ and $B=\frac{2}{3}P^2$, q_1 and q_2 are the phonon momenta denoting the limits of the q integration for energy and momentum conservation, and $L=b_c^2+c_c^2=1-a_c^2$.

For spin-flip scattering one obtains

$$\frac{1}{\tau_{po\downarrow\uparrow}} = \frac{e^2\omega_{\mathrm{LO}}}{8k^2}\left[\frac{1}{\epsilon_\infty}-\frac{1}{\epsilon_s}\right]\frac{[A+B(q_2-k)^2]^{1/2}}{Bk(q_2-k)^2}f \times L^2\left[\tfrac{1}{2}[q_2^2+(q_2-2k)^2](q_2^2-q_1^2)-\tfrac{1}{4}(q_2^4-q_1^4)-q_2^2(q_2-2k)^2\ln\left[\frac{q_2}{q_1}\right]\right] , \tag{B2}$$

where

$$f=\frac{\beta^2}{9}(16\gamma^2+8\beta\gamma+\beta^2) ,$$

and β and γ are defined as in Ref. 28.

---

*On leave from Department of Solid State Physics, Akademia Gorniczo-Hutnicza, aleja Mickiewicza 30, PL-30059 Krakow, Poland.

[1]R. R. Gałazka and J. Kossut, in *Physics of II-VI and I-VII Compounds, Semimagnetic Semiconductors,* Pt. b of *Semiconductors,* Vol. 17 of *Crystal and Solid State Physics,* Gp. 3 of *Landolt-Börnstein, Numerical Data and Functional Relationships in Science and Technology,* New Series, edited by K. H. Hellwege (Springer, Berlin, 1982), p. 302.

[2]I. I. Lyapilin and I. M. Tsidil'kovskii, Usp. Fiz. Nauk **146**, 35 (1985) [Sov. Phys.—Usp. **28**, 349 (1985)].

[3]T. Dietl, Jpn. J. Appl. Phys. **26**, Suppl. 26-3, 1907 (1987).

[4]*Diluted Magnetic Semiconductors,* edited by J. K. Furdyna and J. Kossut, in *Semimetals and Semiconductors,* edited by R. K. Williardson and A. C. Beer (Academic, New York, 1988), Vol. 25.

[5]H. Krenn, W. Zawadzki, and G. Bauer, Phys. Rev. Lett. **55**, 1510 (1985).

[6]H. Krenn, in *Festkörperprobleme (Advances in Solid State Physics),* edited by P. Grosse (Vieweg, Braunschweig, 1986), Vol. 26, p. 183.

[7]D. D. Awschalom, J. Warnock, and S. von Molnar, Phys. Rev. Lett. **58**, 812 (1987).

[8]J. R. Rozen and D. D. Awschalom, Appl. Phys. Lett. **49**, 1649 (1986).

[9]G. Lampel, in *Proceedings of the 12th International Conference on the Physics of Semiconductors,* Stuttgart, 1974, edited by M. H. Pilkuhn (Teubner, Stuttgart, 1974), p. 734, and references therein.

[10]G. Fishman and G. Lampel, Phys. Rev. B **16**, 820 (1977).

[11]C. Herman, Ann. Phys. (Leipzig) **2**, 5 (1977).

[12]D. Paget, G. Lampel, B. Saporal, and V. I. Safarov, Phys. Rev. B **15**, 5780 (1977).

[13]R. Planel, Solid-State Electron. **21**, 1437 (1978).

[14]G. E. Pikus and A. N. Titkov, in *Optical Orientation, Modern Problems in Condensed Matter Sciences,* edited by F. Meyer and B. P. Zacharchenya (North-Holland, Amsterdam, 1986), Vol. 8, p. 73.

[15]T. Dietl and J. Spałek, Phys. Rev. Lett. **48**, 355 (1982); Phys. Rev. **28**, 1548 (1983).

[16]D. Heiman, P. A. Wolff, and J. Warnock, Phys. Rev. B **27**, 4848 (1983).

[17]S. M. Ryabchenko and Yu. G. Semenov, Zh. Eksp. Teor. Fiz. **84**, 1806 (1983) [Sov. Phys.—JETP **57**, 825 (1983)].

[18]R. Planel, Tran Hog Nhung, G. Fishman, and M. Nawrocki, J. Phys. (Paris) **45**, 1071 (1984).
[19]A. Golnik and J. Spałek, J. Magn. Magn. Mater. **54-57**, 1207 (1986).
[20]J. Clarke, in *Superconductor Applications: SQUID's and Machines,* edited by B. B. Schwartz and S. Foner (Plenum, New York, 1977), p. 67.
[21]L. S. Vlasenko, N. V. Zavaritskii, and V. G. Fleisher, Pis'ma Zh. Tekh. Fiz. **9**, 1377 (1983) [Sov. Tech. Phys. Lett. **9**, 592 (1983)].
[22]J. Warnock and D. D. Awschalom, Jpn. J. Appl. Phys. **26**, Suppl. 26-3, 819 (1987).
[23]S. Nagata, R. R. Gałazka, D. P. Mullin, H. Akbarzadeh, G. D. Khattak, J. K. Furdyna, and P. H. Keesom, Phys. Rev. B **22**, 3331 (1980).
[24]H. Krenn, K. Kaltenegger, and G. Bauer, in *Proceedings of the 18th International Conference on the Physics of Semiconductors,* Stockholm, 1986, edited by O. Engström (World Scientific, Singapore, 1987), p. 1477.
[25]H. Krenn, K. Kaltenegger, and G. Bauer, Solid-State Electron. **31**, 481 (1988).
[26]R. R. Parsons, Can. J. Phys. **49**, 1850 (1971).
[27]H. Kahlert and G. Bauer, Phys. Rev. B **7**, 2670 (1973).
[28]W. Zawadzki and W. Szymanska, Phys. Status Solidi B **45**, 415 (1971).
[29]M. I. D'yakonov and V. I. Perel', Fiz. Tverd. Tela **13**, 3581 (1971) [Sov. Phys.—Solid State **13**, 3023 (1972)].
[30]C. Haas, Crit. Rev. Solid-State Sci. **1**, 47 (1970).
[31]Equation (12) is a corrected form of that given in J. Kossut, Phys. Status Solidi B **72**, 359 (1975).
[32]E. O. Kane, J. Phys. Chem. Solids **1**, 249 (1957).
[33]See, e.g., R. J. Nicholas, A. C. Carter, S. Fung, R. A. Stradling, J. C. Portal, and C. Houlbert, J. Phys. C **13**, 5215 (1980).
[34]E. Kartheuser, J. Schmit, and R. Errard, J. Appl. Phys. **63**, 784 (1988).
[35]For a recent discussion of the mean-field approach, see, e.g., T. Dietl, J. Spałek, and L. Swierkowski, Phys. Rev. B **33**, 7303 (1986).
[36]See, e.g., T. Dietl, in *Physics in High Magnetic Fields,* edited by S. Chikazumi and N. Miura (Springer, Berlin, 1981), p. 344.
[37]M. I. D'yakonov and V. I. Perel', Zh. Eksp. Teor. Fiz. **65**, 362 (1973) [Sov. Phys.—JETP **38**, 177 (1974)].
[38]E. A. Harris and K. S. Yngvesson, J. Phys. C **1**, 990 (1968); **1**, 1011 (1968).
[39]D. Scalbert, J. Cernogora, C. Benoît à la Guillaume, Solid State Commun. **66**, 571 (1988).
[40]K. Leibler, A. Sienkiewiccz, K. Checinski, R. R. Gałazka, and A. Pajaczkowska, in *Physics of Narrow-Gap Semiconductors,* edited by J. Rauluszkiewicz *et al.* (Polish Scientific Publishers–PWN, Warszawa, 1978), p. 199.
[41]S. B. Oseroff, Phys. Rev. B **25**, 6584 (1982).
[42]D. J. Webb, S. M. Bhagat, and J. K. Furdyna, J. Appl. Phys. **55**, 2310 (1984).
[43]J. A. Gaj, in *Proceedings of the 17th International Conference on the Physics of Semiconductors,* San Francisco, 1984, edited by J. D. Chadi and W. A. Harrison (Springer, New York, 1984), p. 1423.
[44]J. Warnock, D. Heiman, P. A. Wolff, R. Kershaw, D. Ridgley, K. Dwight, A. Wold, and R. R. Gałazka, in Ref. 42, p. 1407.
[45]V. F. Kovalenko and E. L. Nagaev, Usp. Fiz. Nauk **148**, 561 (1986) [Sov. Phys.—Usp. **29**, 297 (1986)].
[46]S. M. Ryabchenko, Yu. G. Semenov, and O. V. Terletskii, Zh. Eksp. Teor. Fiz. **82**, 951 (1982) [Sov. Phys.—JETP **55**, 557 (1982)].
[47]Yu. G. Semenov, Fiz. Tekh. Poloprovdn. **20**, 1829 (1986) [Sov. Phys.—Semicond. **20**, 1148 (1986)].
[48]G. Bauer and J. Kossut, Phys. Rev. B **31**, 2040 (1985).